CMTC-502924-MS

Pressure Transient Analysis for Characterization of Lateral and Vertical Leakage through Faults

Mojtaba Mosaheb and Mehdi Zeidouni, Louisiana State University

This paper was prepared for presentation at the Carbon Management Technology Conference held in Houston, Texas, USA, 17-20 July 2017.

Abstract

A fault is a potential pathway for fluid leakage, which can contaminate underground water resources. In addition, fault leakage can affect hydrocarbon production. This study aims to develop a type-curve-based methodology to characterize a fault both laterally and vertically using pressure transient analysis. We develop an analytical model to assess the pressure perturbations corresponding to production/injection from/into a reservoir with a leaky fault. Displacement of layers during the fault displacement may cause alteration of the reservoir properties across the fault. This alteration is accounted for by considering different properties on the two sides of the fault. The reservoir is divided into two regions separated by the fault, which are in hydraulic communication with one another and with the overlying/underlying permeable layers. The governing system of differential equations and corresponding boundary conditions are solved using Fourier and Laplace transforms. At early times of the fault leakage, the recorded well pressure changes are mostly affected by the fault properties and the effects of resistance from the upper zone emerge later. In this model, we neglect the resistance to leakage flow caused by the overlying zone to focus on the pressure changes at early times of the fault leakage. We show that these assumptions are

valid to arrive at correct fault characteristics. For fault characterization, type curves are presented in terms of dimensionless vertical and horizontal conductivities of the fault. A computational optimization method is used in combination with type curves to fully characterize the reservoir-fault system. Results show that the characterization method is useful to estimate the fault vertical and lateral conductivities.

Keywords: Analytical model, Characterization, Fault leakage, Pressure transient

Introduction

A fault can cause a discontinuity in formation permeability distorting the fluid flow and may act as a conduit to both lateral and vertical fluid flow. Fault zone permeability may be enhanced or reduced depending on the forces that cause the displacement of the layers and slip location through the fault plane (Sibson, 1977). Faults are generally composed of a core zone surrounded by a damaged zone. The permeability of the core zone is commonly low because this is the location of the slip that the original rock is ground. Compared to the core zone, the surrounding damaged zone's permeability may be enhanced due to possible fractures (Sibson, 1977; Caine et al., 1996). Analogous to the lateral permeability, the vertical permeability of a fault may be enhanced and the fault may be a vertical flow conduit (Maslia and Prowell, 1990). As an example, Bense and Person (2006) investigated the sealing and conductance behaviors of the Baton Rouge Fault in southern Louisiana and showed that the permeability of the fault is enhanced through the fault plane. They also found that the fault permeability is considerably low perpendicular to the fault plane. The existence of faults in underground formations can cause inter-formational fluid migration, particularly affecting water resources (Huntoon and Lundy, 1979). Stoessell and Prochaska (2005) showed that brine from deep saline aquifers migrated upward along the Baton Rouge Fault by several hundreds of meters.

Injection into deep saline aquifers is an industrial method to dispose of unwanted fluids. For instance, CO_2 storage is a method to cut CO_2 atmospheric emissions as a means to mitigate climate change. The injected CO_2 can leak through a nearby fault to shallower aquifers and contaminate the underground water resources (IPCC, 2005). The quality of the underground water resources may change due to CO_2 leakage through local high-permeability pathways such as permeable faults or abandoned wells (Apps et al., 2010). During underground storage of natural gas, migration of injected gas from the target zone through the faults can reduce the accessible gas for reproduction and contaminate underground water resources (Thomas and Benson, 2005). It is of crucial importance to characterize the potential leakage pathways including faults to manage the negative consequences.

In this paper, we investigate characterization of leaky faults based on the pressure transient analysis (PTA).

PTA is an applicable technique to characterize the hydraulic characteristics of the reservoirs based on mathematical modeling of fluid flow in porous media.

Analytical models are especially useful because of their independence of time and space discretization, capability for quick implementation, providing an explicit relationship between the system properties/measurements, and less complex models requiring fewer input of data. Several mathematical methods were used to present analytical solutions for fluid flow in a system including a fault as a discontinuity. Integral transforms (Bixel et al., 1963), Laplace-Fourier transformation (Ambastha et al., 1989), and Green's function (Raghavan, 2010) are examples of the mathematical solution methods. Analytical approaches to modeling a faulted system are reviewed in the following.

Bixel et al. (1963) investigated the transient pressure behavior of a well located near a fault and proposed an analytical solution based on the integral transforms. Stewart and Gupta (1984) investigated interference testing in a reservoir including a non-sealing fault and introduced drawdown type curves using numerical simulation approach. The pressure discontinuity across the fault was shown by Yaxley (1987). He obtained an analytical solution for pressure transient behavior of a vertical non-sealing barrier. The reservoir properties of two sides of the fault were assumed identical. Ambastha et al. (1989) presented an analytical solution with different reservoir properties at two sides of the fault. They demonstrated that the results of the interference tests are influenced by the property contrasts of the composite system and the location of the observation well. Rahman et al. (2003) presented an analytical solution to the transient flow problem of a system of two regions with a finite conductivity fault. The solution accounts for the transient flow within the fault. They concluded that the effect of transient flow in the fault can be negligible.

Modeling of the vertical leakage through the fault has received attention more recently. Shan et al. (1995) incorporated the effect of vertical leakage to an upper permeable zone in the suggested analytical model. However, they ignored the pressure discontinuity through the fault in the injection layer. Zeidouni (2012) presented analytical solutions of two-layer and multi-layer systems, which demonstrated the pressure discontinuity through the fault in presence of vertical leakage. Zeidouni (2016) extended the multi-layer solution for a leaky fault by fully accounting for the lateral resistance of the fault in all layers. Many other works have been done to address fluid leakage from a target zone (Pruess, 2005; Ebigbo et al., 2007; Birkholzer et al., 2009; Humez et al., 2011; Zeidouni and Pooladi-Darvish, 2012; Shakiba and Hosseini, 2016; Mosaheb and Zeidouni, 2017a, b).

The main goal of this study is to present type curves for fault characterization and demonstrate how they can be used to determine fault lateral and vertical conductivities. In obtaining the analytical solution, we build on an existing analytical solution by Zeidouni (2012). we neglect the resistance to flow caused by

the overlying/underlying formations to reduce the number of parameters required to characterize the system. A fault usually intersects a sequence of adjacent permeable layers, which can be represented, by a single thick zone with high flow capacity (permeability×thickness). The superposition of the numerous overlying/underlying layers may show no resistance to vertical flow, especially at early times of leakage. The validity of this assumption is investigated as described in the next paragraph. In addition, unlike Zeidouni (2012, 2016), the flow capacities in the injection zone are considered different at two sides of the fault, allowing for possible layer juxtaposition.

In the following, we first present the physical system followed by corresponding analytical model. The analytical solution is verified against numerical simulation results. The analytical solution is cast in the form of type curves that can be readily applied to characterize lateral and vertical conductivity of the fault. Due to the large number of dimensionless groups obtained by the analytical solution, the system cannot be fully characterized using the type curves alone. We present a computational optimization method in combination with type curves to fully characterize the reservoir-fault system. Our approach is based on estimating the dimensionless parameters that describe the hydraulic properties of the fault and the altered region on the other side of the fault. Finally, we apply our proposed method to two example problems.

Analytical model

For the physical system to be modeled, the target zone is separated into two regions (region 1 and region 2) by a vertical planar fault. Region 1 is on the side of the fault where the active well is located and region 2 is on the opposite side of the fault (Fig. 1). Because of possible displacement of the layers on the two sides of the fault plane, the thickness and reservoir properties of region 2 may be different from those of region 1. The reservoir properties are homogeneous and isotropic at each region. The y-axis is horizontal and perpendicular to the x-axis. The active well is assumed to be a line source/sink and is perforated over the whole thickness of the reservoir at $x=a$ and $y=0$ in the target zone. The reservoir is initially saturated with a single-phase fluid and the injected fluid is the same as the initial fluid. Both the upper zone and the target zone are infinite at both sides of the x and y axes. The fault plane is perpendicular to the x-axis, and it is located at $x=0$. The fault allows flow communications between region 1, region 2, and the upper zone. The horizontal and vertical permeabilities of the fault are considered constant.

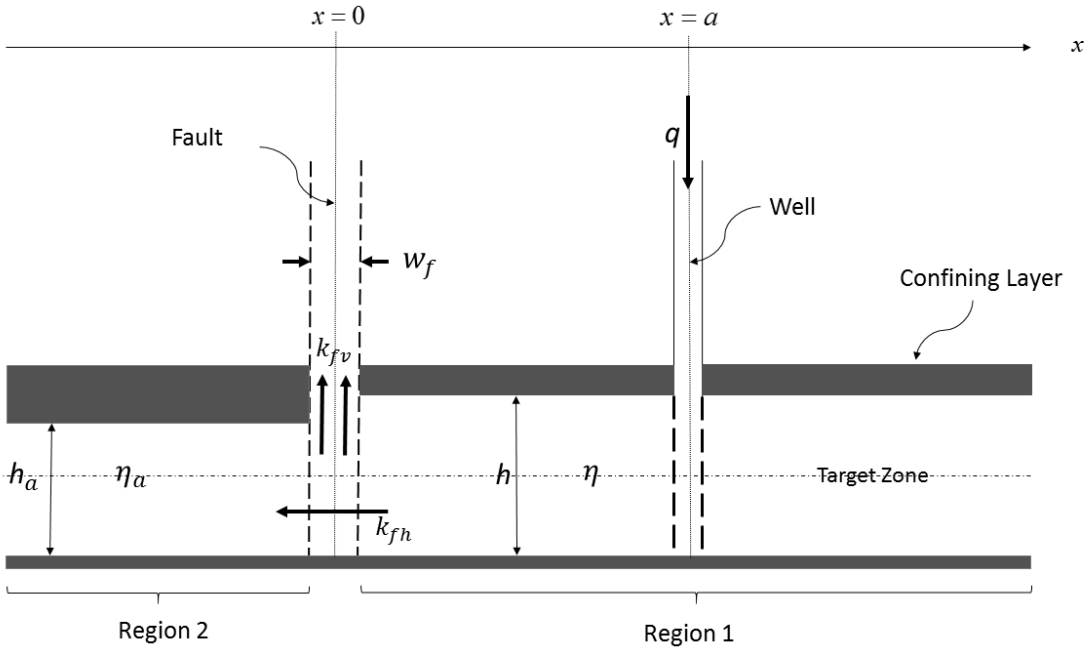

Fig. 1 Schematic representation of the physical model

The diffusivity equations for regions 1 and 2 make a system of two linear differential equations. The pressure change of the upper zone is negligible because the flow capacity of that zone is assumed to be large. Equations (1)-(10) represent diffusivity equations of regions 1 and 2 and the corresponding initial and boundary conditions:

Region 1:

$$\frac{\partial^2 \Delta P_1}{\partial x^2} + \frac{\partial^2 \Delta P_1}{\partial y^2} + \frac{q\mu}{kh}\delta(x-a)\delta(y) = \frac{1}{\eta}\frac{\partial \Delta P_1}{\partial t} \tag{1}$$

$$\Delta P_1(x, y, 0) = 0 \tag{2}$$

$$\Delta P_1(x, \pm\infty, t) = 0 \tag{3}$$

$$\Delta P_1(+\infty, y, t) = 0 \tag{4}$$

$$\frac{kh}{\mu}\frac{\partial \Delta P_1(0, y, t)}{\partial x} = \frac{k_{fh}h}{\mu w_f}(\Delta P_1(0, y, t) - \Delta P_2(0, y, t)) + \frac{k_{fv}w_f}{2\mu L}(\Delta P_1(0, y, t)) \tag{5}$$

Region 2:

$$\frac{\partial^2 \Delta P_2}{\partial x^2} + \frac{\partial^2 \Delta P_2}{\partial y^2} = \frac{1}{\eta_a}\frac{\partial \Delta P_2}{\partial t} \tag{6}$$

$$\Delta P_2(x, y, 0) = 0 \tag{7}$$

$$\Delta P_2(x, \pm\infty, t) = 0 \tag{8}$$

$$\Delta P_2(-\infty, y, t) = 0 \tag{9}$$

$$\frac{k_a h_a}{\mu}\frac{\partial \Delta P_2(0,y,t)}{\partial x}+\frac{k_{fv} w_f}{2\mu L}(\Delta P_2(0,y,t))=\frac{k_{fh} h}{\mu w_f}(\Delta P_1(0,y,t)-\Delta P_2(0,y,t)) \tag{10}$$

where L is half thickness of the above zone. The system of partial differential equations and the corresponding initial and boundary conditions (Equations (1)-(10)) are simplified to a system of ordinary differential equations using a combination of Laplace and Fourier transforms. Equations (11)-(12) state the sequence of applying Laplace and Fourier transforms to time and space domains:

$$\overline{\Delta P}(x,y,s)=\mathcal{L}\left[\Delta P(x,y,t)\right]=\int_0^{\infty}\Delta P(x,y,t)e^{-st}dt \tag{11}$$

$$\overline{\overline{\Delta P}}(x,\omega,s)=\mathcal{F}\left[\overline{\Delta P}(x,y,s)\right]=\int_{-\infty}^{+\infty}\overline{\Delta P}(x,y,s)e^{i.\omega.y}dy \tag{12}$$

where s and ω are Laplace and Fourier transform dummy variables, respectively. Equations (13)-(14) provide the final solution of the pressure distribution at region 1 and region 2, respectively in dimensionless form (the solution details are given in the Appendix). The Laplace-Fourier domain is shown by = on the pressure (Equation (12)) and dimensionless pressure (Equations (13)-(14)).

$$\bar{\bar{P}}_{D1}=\frac{1}{2sA_1}\left(e^{-A_1|x_D-1|}+\frac{A_1\alpha-A_1\alpha_u-2\alpha\alpha_u-\alpha_u{}^2+A_1A_2T_D-A_2T_D\alpha-A_2T_D\alpha_u)}{A_1\alpha+A_1\alpha_u+2\alpha\alpha_u+2\alpha_u+A_1A_2T_D+A_2T_D\alpha+A_2T_D\alpha_u}e^{-A_1(x_D+1)}\right) \tag{13}$$

$$\bar{\bar{P}}_{D2}=\frac{\alpha}{s}\times\left(\frac{1}{A_1\alpha+A_1\alpha_u+2\alpha\alpha_u+2\alpha_u+A_1A_2T_D+A_2T_D\alpha+A_2T_D\alpha_u}e^{(-A_1+A_2x_D)}\right) \tag{14}$$

where:

$$P_{D1}=\frac{kh}{q\mu}\Delta P_1\ ,\ P_{D2}=\frac{kh}{q\mu}\Delta P_2\ ,\ t_D=\frac{\eta t}{a^2}\ ,\ x_D=\frac{x}{a}\ ,\ y_D=\frac{y}{a} \tag{15}$$

$$\alpha=\left(\frac{k_{fh}(h+h_a)}{2w_f}\right)\Big/\left(\frac{kh}{a}\right),\quad \alpha_u=\left(\frac{k_{fv}w_f}{2L}\right)\Big/\left(\frac{kh}{a}\right) \tag{16}$$

$$T_D=\frac{k_a h_a}{kh}\ ,\ \eta_D=\frac{\eta_a}{\eta} \tag{17}$$

$$A_1{}^2=\omega^2+s\ ,\ A_2{}^2=\omega^2+\frac{s}{\eta_D} \tag{18}$$

where w_f, k_{fv}, and k_{fh} are the fault width and vertical and horizontal permeability of the fault, respectively. α and α_u are dimensionless horizontal and vertical conductivities of the fault and t_D is dimensionless time. T_D and η_D are flow capacity and diffusivity ratios, respectively. The solution must be inverted from the Laplace-Fourier domain to time-space domain. Analytical inversion of the solution to a closed-form

solution in the time-space domain is impossible. Therefore, numerical Laplace and Fourier inversion methods are used to obtain the solution in time-space domain. Stehfest algorithm (Stehfest, 1970) is used for Laplace inversion and the Inverse Discrete Fourier Transform (IDFT) is used for Fourier inversion.

Verification of the analytical model

The analytical solution is verified by comparison of spatial and temporal variation of the pressure with the numerical simulation results. In dimensional terms (corresponding to the dimensional values), the width of the fault is 0.1 m, the porosity is 0.2, total compressibility factor is 1×10^{-6} 1/kPa, and injection rate is 0.005 m^3/s. The reservoir thickness and permeability of region 1 are 10 m and 10 mD, respectively. Fault lateral and vertical permeabilities are 0.01 mD and 5000 mD, respectively. The system specifications are given in Table 1. Fig. 2 exhibits the pressure distribution on the line drawn through the well perpendicular to the fault plane. The lateral pressure discontinuity is visible across the fault, which shows that the lateral permeability of the fault is less than the reservoir permeability. Fig. 2 illustrates that the analytical solution is in good agreement with the numerical simulation at both regions 1 and 2. If there is no lateral leakage, the pressure in region 2 remains constant at initial pressure. Therefore, the pressure gradient along region 2 shown in Fig. 2 (from x=-100 to x=0) is a sign of lateral leakage through the fault.

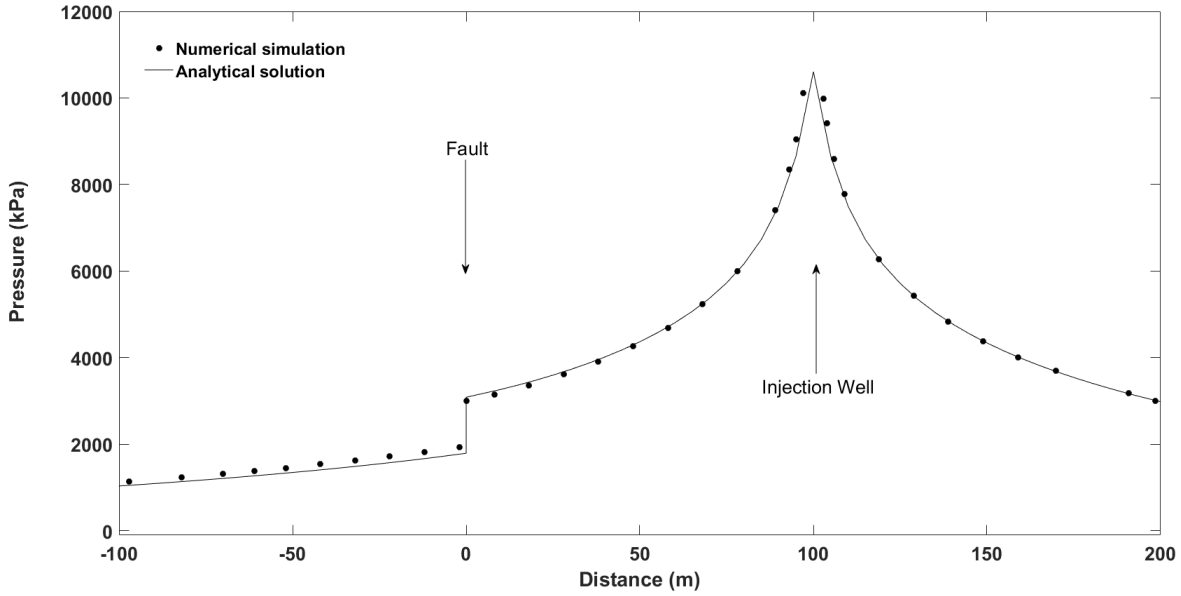

Fig. 2 Validation of the spatial pressure distribution in the injection zone after 10 days.

Fig. 3 illustrates good agreements of pressure and logarithmic pressure derivative (referred to as derivative hereafter) between analytical and numerical simulation. The verification of the pressure derivative is important because the characterization method to be presented later is based on the pressure

derivative curves.

Table 1. Reservoir properties

Parameter	Value	Parameter	Value
Effective width of the fault (m)	0.1	Viscosity (cp)	0.5
Lateral permeability of the fault (mD)	0.01	Injection rate ($m^3.s^{-1}$)	0.005
Vertical permeability of the fault (mD)	5000	Total compressibility (1/kPa)	10^{-6}
Target zone thickness (m)	10	fault vertical conductivity , α_u	0.12
Fault-well Distance (m)	100	fault lateral conductivity , α	1
Permeability of region 1 (mD)	10	Diffusivity ratio , η_D	1
Permeability of region 2 (mD)	10	Flow capacity ratio , T_D	1
Porosity (fraction)	0.2		

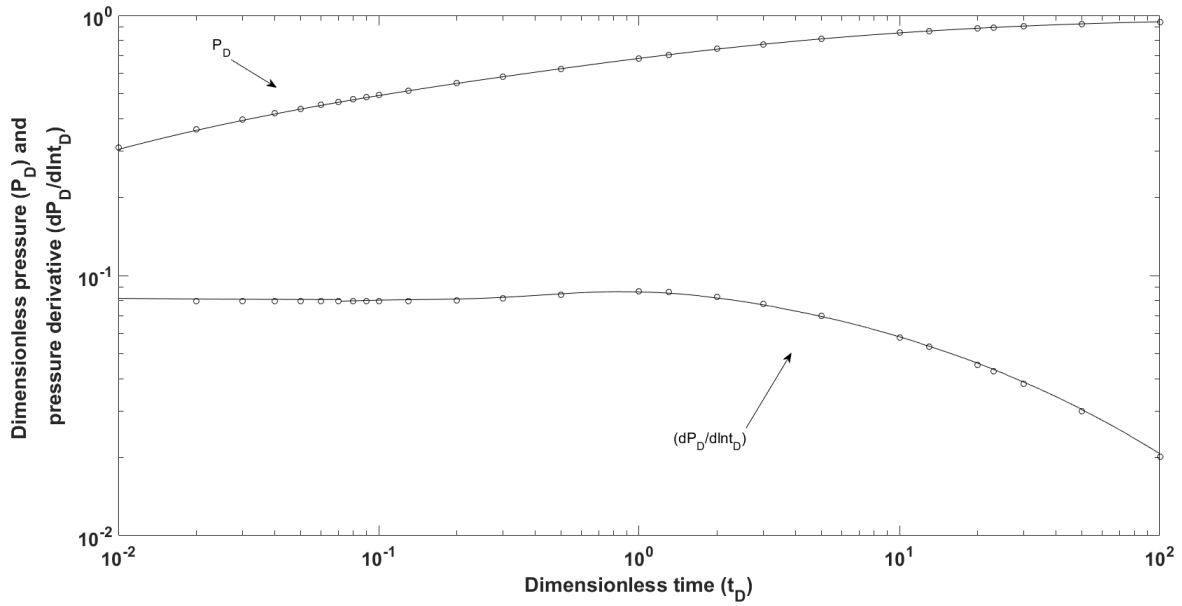

Fig. 3: Validation of temporal variation of well pressure and (logarithmic) pressure derivative with respect to time using numerical simulation

Fault characterization

In this section, type curves are introduced for characterization of the leaky fault. Type curves are generalized and adjusted in terms of dimensionless variables. Based on the analytical solution, the reservoir-fault system can be characterized by four groups: Fault lateral and vertical conductivities, reservoir flow capacity ratio, and diffusivity ratio. These four groups are represented by dimensionless parameters: α, α_u, T_D, and η_D, respectively. The characterization procedure is presented based on the type curves.

Type curves

Fig. 4 illustrates the type curves corresponding to the leaky fault system in terms of fault lateral (α) and vertical (α_u) conductivities for T_D =η_D=1. We refer to type curves of Fig. 4 as the base type curves. The type curves are grouped for various values of α_u. At each group, α varies from zero to infinity. The negative unit slope line of the logarithmic derivative curves in Fig. 4 shows the early time of the vertical leakage. The negative unit slope line would occur before appearance of flow resistance from the overlying/underlying zone. Using these type curves, hydraulic characteristics of the fault can be estimated with the well pressure data before detecting any resistance from the overlying/underlying zones.

A well pressure data corresponding to unique values of α and α_u would match with a unique type curve. In finding the matching type curve, α_u is easier to obtain from late time pressure data while parameter α is easier to estimate using early time data. Implementing this technique of using the early time and the late time data separately can help in resolving the choice of intermediate values of α and α_u. In other words, for two close values of α_u, the two corresponding groups of type curves may be very close to one another at late time, but the two curves should deviate from each other at early time curvature making it easy to recognize which one belongs to which group. In addition, two curves with too close values of α and different values of α_u may be close to each other at the early time. Then, their late time deviation can be used to determine the correct type curve. In short, there is a unique type curve for each combination of α_u and α which should be easy to be distinguished from the other curves. In addition, the point when deviation from the radial flow (the zero-slope derivative line prior to reaching the fault) would commence are useful to find the best matching type curve.

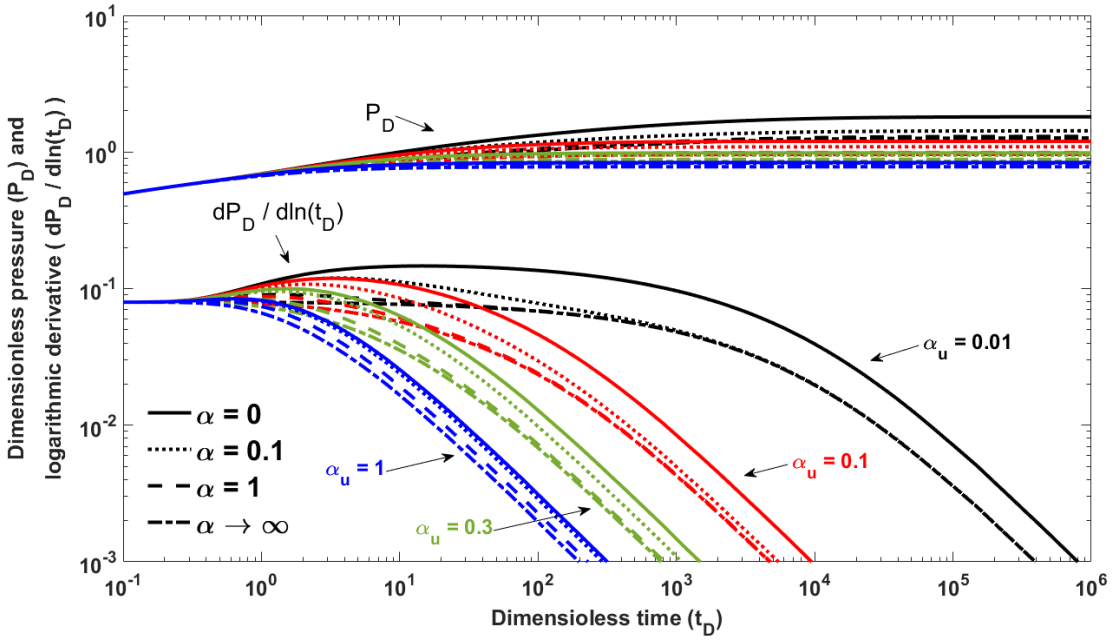

Fig. 4: Type curves of the leaky fault system considering T_D=1 and η_D=1

In order to use these type curves, the well pressure data should be plotted versus time in the same scale as the type curves on a transparent plot. The resulting plot should be next moved horizontally and vertically (without rotation) to find the best match with the type curves to estimate α and α_u. In addition to α and α_u, region 1 permeability and fault-well distance can also be evaluated based on the radial flow prior to reaching the fault. By selecting an arbitrary match point, we get $(P_D)_M$, $(\Delta P)_M$, $(t)_M$, and $(t_D)_M$ of that match point to calculate region 1 permeability (k) and fault-well distance (a) based on Equations (19) and (20).

$$k = \frac{q\mu}{h}\left(\frac{P_D}{\Delta P}\right)_M \tag{19}$$

$$a = \sqrt{\eta\left(\frac{t}{t_D}\right)_M} \tag{20}$$

One observation from these type curves is that 2 to 3 log-cycles of data may be required for identification of the fault characteristics. This implies that if the fault is felt after 1 hr test, 10 to 100 hrs of test may be required to enable characterizing of the fault. The type curves can be extended to determine T_D and η_D as well. Fig. 5 illustrates the effect of T_D and η_D on the pressure and pressure derivative for a fixed value of α (=0.1). The effect of T_D and η_D is most visible at the lowest values of α_u. Similar patterns are achieved for different values of α.

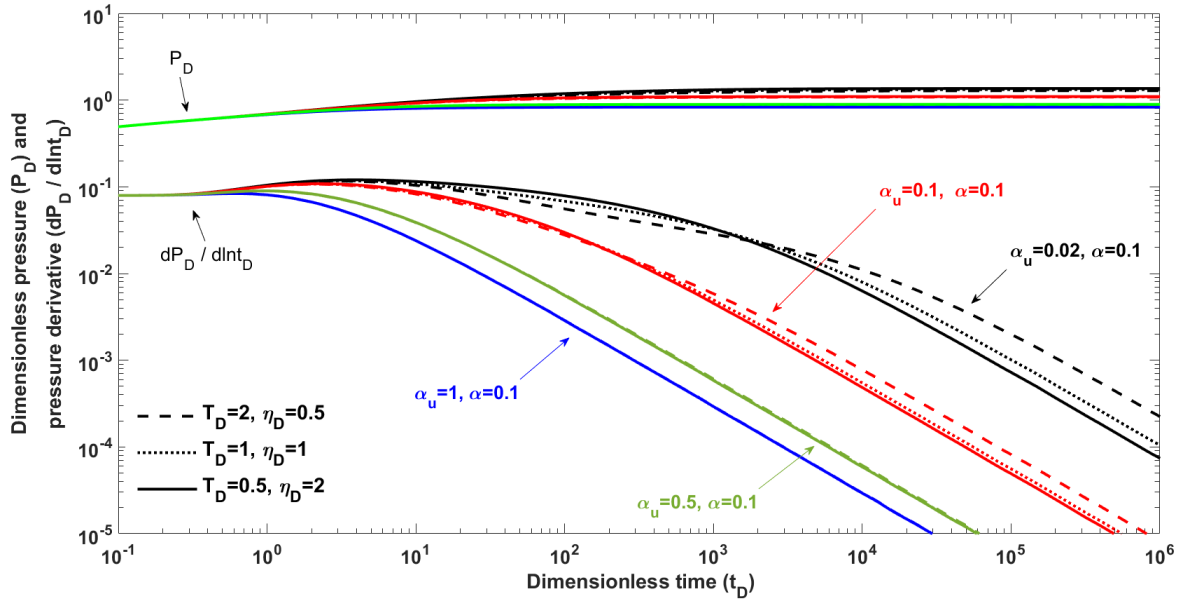

Fig. 5 Effect of T_D and η_D on the type curves

Fig. 5 shows that by increasing α_u, the sensitivity of the pressure derivative curve to the parameters T_D

and η_D will decrease. In the following, we introduce a procedure to estimate the dimensionless parameters. First, initial values of α and α_u are estimated by the base type curves. Next, an optimization method is applied to find the accurate values of the dimensionless parameters using the initial values obtained from type curve analysis. We use the MATLAB built-in optimization tool given by the *fmincon* optimization function (Matlab, 2015). This function is based on a sequential quadratic programming, which is a gradient-based algorithm. Here, fmincon optimization is applied to minimize the square of the difference between well pressure data and the mathematical solution by changing the four dimensionless parameters.

Characterization procedure

In characterization procedure, first, we estimate the initial values of α and α_u from the type curves. Next, we calculate the values of permeability and fault-well distances using Equations (19) and (20). In the optimization process, we use the pressure data to modify the estimated initial value of α and α_u. Next, we fix T_D and η_D. This step is done by the late time data because T_D and η_D have a negligible effect on the early time data. The initial values of T_D and η_D can be considered equal to one. This sequential procedure improves the optimization process compared to optimizing all four dimensionless parameters simultaneously using the whole pressure data. The characterization procedure is summarized in Fig. 6.

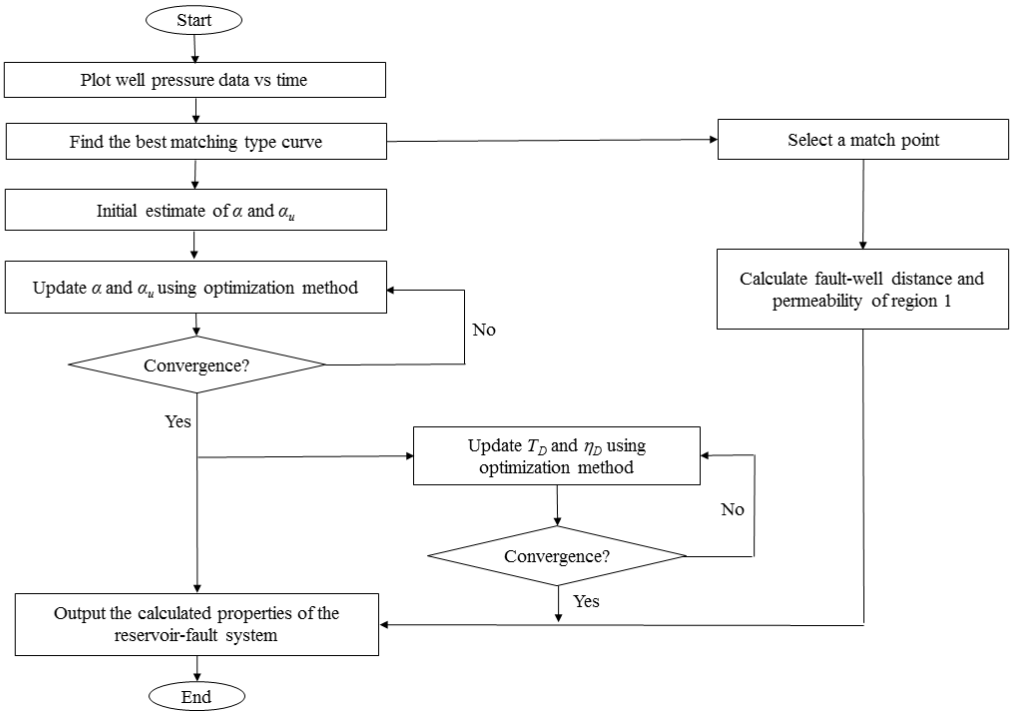

Fig. 6 Characterization procedure of the leaky fault system

Results and discussion

In this part, two examples are presented to estimate fault characteristics by the type-curve method using the procedure described in the previous section.

Example 1: No alteration of reservoir properties across the fault

In this example, we analyze the well pressure data of an injection well near a fault. The permeability, porosity, total compressibility, and thickness of the target zone at both sides of the fault are respectively 100 mD, 0.1, 10^{-6} 1/kPa, and 10 m. The flow capacity of the upper zone is large enough compared to the injection zone. The injection rate is 0.005 $m^3.s^{-1}$ and fluid viscosity is 0.5 cp. Fig. 7 shows the synthetic well pressure data and pressure derivative of the first example in which α and α_u are considered 1 and 0.3, respectively. These values correspond to 62 D and 0.1 mD for vertical and horizontal permeabilities of the fault considering a 0.1-m wide fault. Fluid leakage through the fault can be inferred from the derivative curve. If the fault is sealing, the pressure derivative becomes zero-slope after departing from the zero-slope corresponding to initial radial flow (Fig. 8). The late time horizontal line in Fig. 8 exhibits the pressure response of a sealing fault in which α and α_u are equal to zero.

The pressure data and the derivative are required on a plot with the same scale as the type curves for type-curve matching. Fig. 9 shows the type curve that best agrees with the pressure data. Corresponding values of α and α_u are estimated for the fault. The estimated values of α and α_u are 1 and 0.3, which are the true values used in generating our synthetic data. By selecting an arbitrary match point and using equations (19) and (20), the permeability of region 1 and the fault-well distance can be calculated as below:

$$(P_D)_M = 0.08 \ , \ (\Delta P)_M = 199 \ \ kPa \ , \ (t_D)_M = 0.07 \ , \ (t)_M = 1000 \ \ s \tag{21}$$

$$k = \frac{q\mu}{h}\left(\frac{P_D}{\Delta P}\right)_M = \ 100.5 \text{ mD} \tag{22}$$

$$a = \sqrt{\eta\left(t/t_D\right)_M} = 100.2 \ \text{ m} \tag{23}$$

These values are in close agreement with the correct values (k=100 mD, a=100 m).

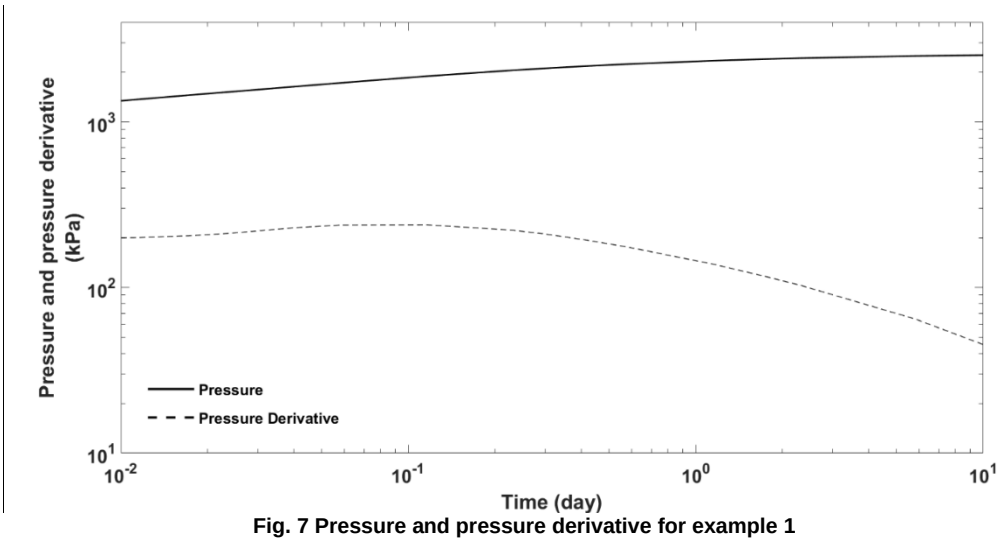

Fig. 7 Pressure and pressure derivative for example 1

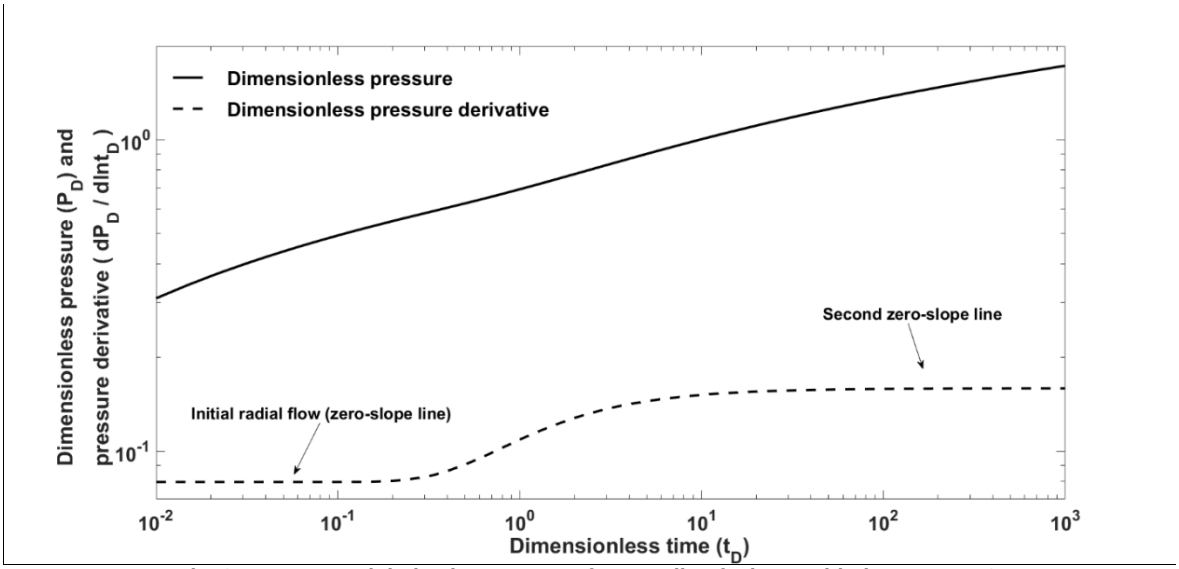

Fig. 8 Pressure and derivative response for a sealing fault, considering $\alpha = \alpha_u = 0$.

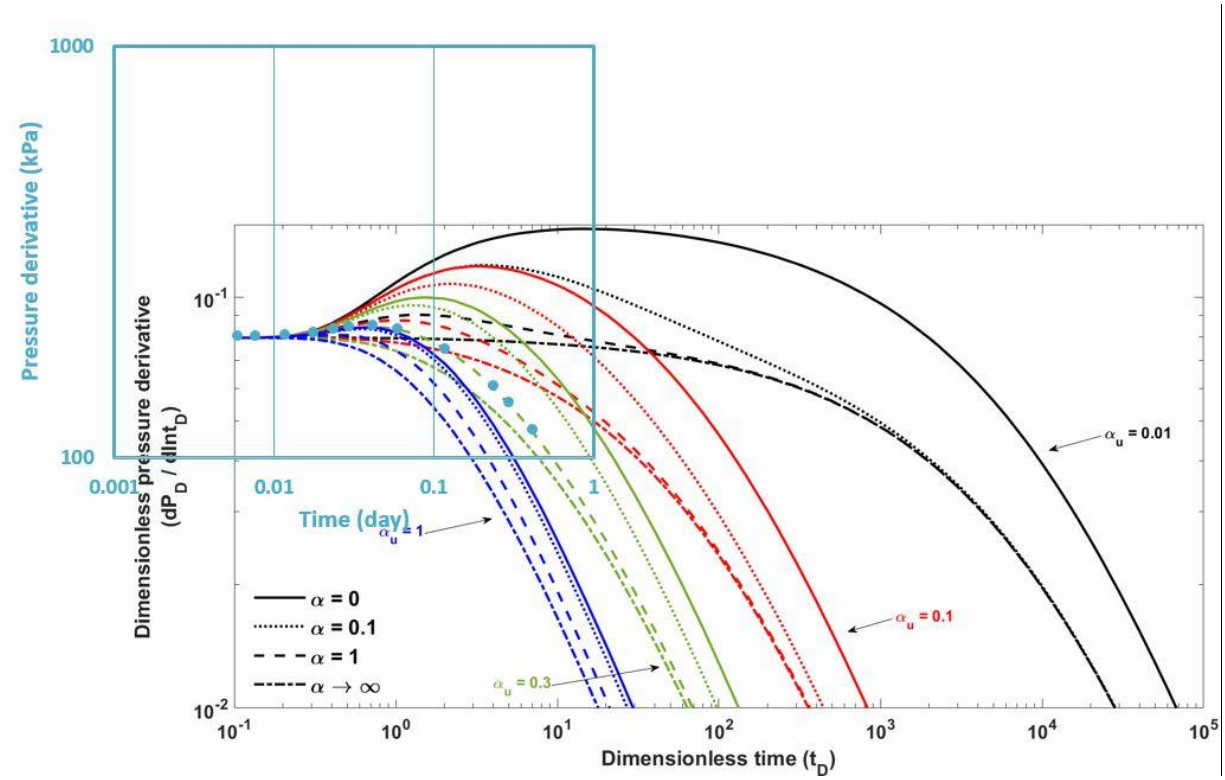

Fig. 9 Estimating α and α_u with the type curves for example 1

Example 2: Alteration of reservoir properties across the fault

Fig. 10 shows the synthetic pressure data of an injection well near a fault in which α, α_u, T_D, and η_D are considered 0.02, 0.5, 0.1, and 0.1 respectively. The flow capacity of the upper zone is large in proportion to the injection zone. In this example, we characterize the leaky fault while the reservoir properties of region 2 may not be identical to those of region 1. The injection rate is 0.005 $m^3.s^{-1}$, the viscosity is 0.5 cp, the porosity is 0.1, total compressibility is 10^{-6} 1/kPa, and reservoir thickness is 20 m. First, we use the base type curves to find the initial values for α and α_u. In this case, the pressure data curve may not accurately match with the type curves but we try to find the best match. The best match of the pressure data with the type curves is illustrated in Fig. 11. The estimated initial values of α and α_u are 0.2 and 0.03, respectively.

When $T_D \neq 1$ and/or $\eta_D \neq 1$, the effects of T_D and η_D on the pressure derivative curve appear after the arrival of the pressure pulse to the fault. The variations of T_D and η_D will not affect the early time pressure data. Thus, similar to example 1, we can select an arbitrary match point to estimate the fault-well distance and permeability of region 1 (Equations (24)-(26)).

$$(P_D)_M = 0.098\ ,\ (t_D)_M = 1\ ,\ \ (t_D)_M = 1\ ,\ (t)_M = 10022\ \text{s} \tag{24}$$

$$k = \frac{q\mu}{h}\left(\frac{P_D}{\Delta P}\right)_M = 49.4 \text{ mD} \tag{25}$$

$$a = \sqrt{\eta\left(t/t_D\right)_M} = 100.1 \text{ m} \tag{26}$$

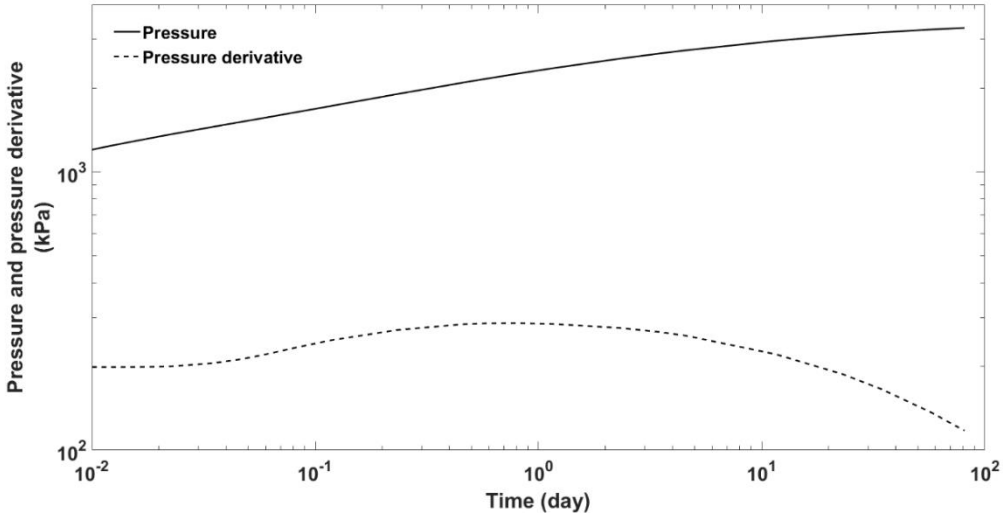

Fig. 10 Pressure and derivative data for example 2

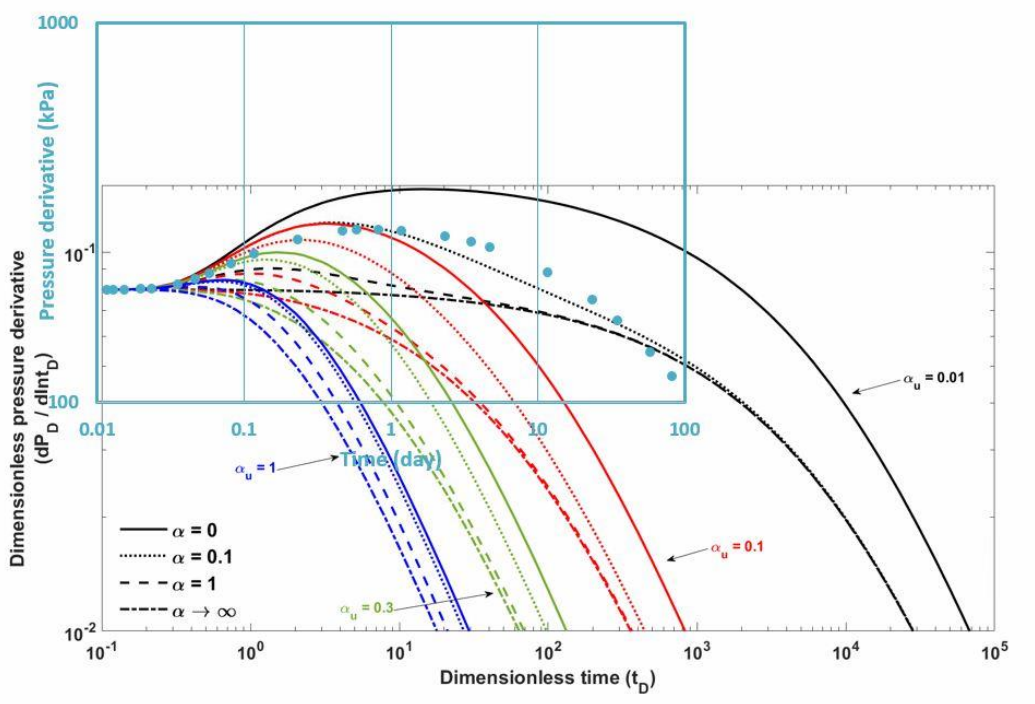

Fig. 11 Estimation of α and α_u with the base type curves for example 2

Next, the optimization method is used to find accurate values of the dimensionless parameters. We set the initial values of T_D and η_D equal to one. The calculated permeability and fault-well distance (k and a)

are used to convert the well pressure data to dimensionless numbers. We apply optimization function to find the best match between the dimensionless pressure data and the analytical solution by modifying the four dimensionless parameters. Using the optimization method, the estimated values of the dimensionless parameters are α=0.5, α_u=0.02, T_D=0.1 and η_D=0.29. The estimated values of fault conductivities (α and α_u) are true values corresponding to synthetic data. Generally, effects of fault conductivities on the pressure derivative are more than effects of diffusivity and flow capacity ratios in this model. Because the model is focused on the early times of fault leakage.

Conclusions

In this study, we preseted a type-curve based method to characterize a vertically and laterally leaking fault using pressure data. In order to develop the type curves, we developed an analytical solution. The reservoir properties on the two sides of the fault are considered non-identical. The analytical solution was verified against the numerical simulation results. In this model, we neglect the resistance to flow by overlying/underlying permeable layers connected to the reservoir by the fault. We investigated the validity of this assumption by assigning different flow capacities to the overlying/underlying zones. This assumption is valid before reaching to the effects of the adjacent zone. The model was cast in the form of type curves to characterize lateral and vertical leakage through the fault. We used the optimization method in combination with the type curves to identify α, α_u, T_D, and η_D. The type curves were used to find the initial values of unknown parameters. Applying the optimization method, very accurate values of α_u and α were estimated by modifying the initial values. As α_u increased, the sensitivity of the pressure response to T_D and η_D was reduced. However, for low values of α_u, the well pressure data were considerably sensitive to T_D and η_D. The sensitivity of this range of pressure data on flow capacity and diffusivity ratios (T_D and η_D) is less than that to the fault vertical and lateral conductivities. This work shows that the pressure data prior to reaching the flow resistance of the overlying/underlying zone can be enough to estimate hydraulic characteristics of the leaky fault.

Acknowledgement

This study was partially supported by the Louisiana Board of Regents under contract #43950.

Appendix: Mathematical solution

We present the system of differential equations in dimensionless form for generality and convenience. The system of differential equations of regions l and 2 and the corresponding boundary conditions (Equations (1)-(10)) are converted to dimensionless form using Equations (15)-(17).

Region 1:

$$\frac{\partial^2 P_{D1}}{\partial x_D^2}+\frac{\partial^2 P_{D1}}{\partial y_D^2}+\delta(x_D-1)\delta(y_D)=\frac{\partial P_{D1}}{\partial t_D} \tag{A1}$$

$$P_{D1}(x_D,y_D,0)=0 \tag{A2}$$

$$P_{D1}(x_D,\pm\infty,0)=0 \tag{A3}$$

$$P_{D1}(+\infty,y_D,t_D)=0 \tag{A4}$$

$$\frac{\partial P_{D1}(0,y_D,t_D)}{\partial x_D}=\alpha(P_{D1}(0,y_D,t_D)-P_{D2}(0,y_D,t_D))+\alpha_u(P_{D1}(0,y_D,t_D)) \tag{A5}$$

Region 2:

$$\frac{\partial^2 P_{D2}}{\partial x_D^2}+\frac{\partial^2 P_{D2}}{\partial y_D^2}=\frac{1}{\eta_D}\frac{\partial P_{D2}}{\partial t_D} \tag{A6}$$

$$P_{D2}(x_D,y_D,0)=0 \tag{A7}$$

$$P_{D2}(x_D,\pm\infty,t_D)=0 \tag{A8}$$

$$P_{D2}(-\infty,y_D,t_D)=0 \tag{A9}$$

$$T_D\frac{\partial P_{D2}(0,y,t)}{\partial x_D}+\alpha_u(P_{D2}(0,y,t))=\alpha(P_{D1}(0,y,t)-P_{D2}(0,y,t)) \tag{A10}$$

To solve the system of differential equations, the method of Laplace and Fourier transforms is used. Applying the transforms, the system of partial differential equations in time-space domain is converted into a system of ordinary differential equations in Laplace-Fourier domain that can be solved. Then, the solutions should be converted back to the time-space domain using Laplace-Fourier inverse transforms. The Laplace transform of the function P_D is defined as below:

$$\overline{P_D}(x_D,y_D,s)=\mathcal{L}[P_D(x_D,y_D,t_D)]=\int_0^\infty P_D(x_D,y_D,t_D)e^{-st_D}dt_D \tag{A11}$$

where s is the Laplace transform variable. First, the Laplace transform is applied into the time domain.

Region 1:

$$\frac{\partial^2 \bar{P}_{D1}}{\partial x_D^2} + \frac{\partial^2 \bar{P}_{D1}}{\partial y_D^2} + \frac{1}{s}\delta(x_D - 1)\delta(y_D) = s\bar{P}_{D1} \tag{A12}$$

$$\bar{P}_{D1}(x_D, \pm\infty, s) = 0 \tag{A13}$$

$$\bar{P}_{D1}(+\infty, y_D, s) = 0 \tag{A14}$$

$$\frac{\partial \bar{P}_{D1}(0, y_D, s)}{\partial x_D} = \alpha(\bar{P}_{D1}(0, y_D, s) - \bar{P}_{D2}(0, y_D, s)) + \alpha_u(\bar{P}_{D1}(0, y_D, s)) \tag{A15}$$

Region 2:

$$\frac{\partial^2 \bar{P}_{D2}}{\partial x_D^2} + \frac{\partial^2 \bar{P}_{D2}}{\partial y_D^2} = \frac{s}{\eta_D}\bar{P}_{D2} \tag{A16}$$

$$\bar{P}_{D2}(x_D, \pm\infty, s) = 0 \tag{A17}$$

$$\bar{P}_{D2}(-\infty, y_D, s) = 0 \tag{A18}$$

$$T_D \frac{\partial \bar{P}_{D2}(0, y_D, s)}{\partial x_D} + \alpha_u(\bar{P}_{D2}(0, y_D, s)) = \alpha(\bar{P}_{D1}(0, y_D, s) - \bar{P}_{D2}(0, y_D, s)) \tag{A19}$$

The Fourier transform of function $\overline{P_D}$ is defined as below:

$$\overline{\overline{P_D}}(x_D, \omega, s) = \mathcal{F}[\overline{P_D}(x_D, y_D, s)] = \int_{-\infty}^{+\infty} \overline{P_D}(x_D, y_D, s) e^{i.\omega.t} dt \tag{A20}$$

where ω is the Fourier parameter. Second, the Fourier transform is applied into the space domain (y_D) and the ordinary system of differential equations and corresponding boundary conditions in the Laplace-Fourier domain is obtained:

Region 1:

$$\frac{d^2 \bar{\bar{P}}_{D1}}{dx_D^2} - A_1^2 \bar{\bar{P}}_{D1} = -\frac{1}{s}\delta(x_D - 1) \tag{A21}$$

$$\bar{\bar{P}}_{D1}(+\infty) = 0 \tag{A22}$$

$$\frac{\partial \bar{\bar{P}}_{D1}(0)}{\partial x_D} = \alpha(\bar{\bar{P}}_{D1}(0) - \bar{\bar{P}}_{D2}(0)) + \alpha_u(\bar{\bar{P}}_{D1}(0)) \tag{A23}$$

Region 2:

$$\frac{d^2\bar{\bar{P}}_{D2}}{dx_D^2} - A_2{}^2\bar{\bar{P}}_{D2} = 0 \tag{A24}$$

$$\bar{\bar{P}}_{D2}(-\infty) = 0 \tag{A25}$$

$$T_D\frac{\partial\bar{\bar{P}}_{D2}(0)}{\partial x_D} + \alpha_u(\bar{\bar{P}}_{D2}(0)) = \alpha(\bar{\bar{P}}_{D1}(0) - \bar{\bar{P}}_{D2}(0)) \tag{A26}$$

where $A_1=\omega^2+s$ and $A_2=\omega^2+s/\eta_D$. The solution in Laplace-Fourier domain is as below.

Region 1:

$$\bar{\bar{P}}_{D1} = \frac{1}{2sA_1}\left(e^{-A_1|x_D-1|}\right) + C_1e^{-A_1x_D} \tag{A27}$$

$$C_0A_1 - C_1A_1 = \alpha(C_0 + C_1 - C_2) + \alpha_u(C_0 + C_1) \tag{A28}$$

Region 2:

$$\bar{\bar{P}}_{D2} = C_2e^{A_2x_D} \tag{A29}$$

$$T_DC_2A_2 + C_2\alpha_u = \alpha(C_0 + C_1 - C_2) \tag{A30}$$

where $C_0 = (1/(2sA_1))e^{-A_1}$. C_1 and C_2 are unknown constants, which must be calculated by combining the equations (A28) and (A30). The solutions for dimensionless pressure of regions 1 and 2 in Laplace-Fourier domain are:

$$\bar{\bar{P}}_{D1} = \frac{1}{2sA_1}\left(e^{-A_1|x_D-1|} + \frac{A_1\alpha + A_1\alpha_u - 2\alpha\alpha_u - \alpha_u{}^2 + A_1A_2T_D - A_2T_D\alpha - A_2T_D\alpha_u}{A_1\alpha + A_1\alpha_u + 2\alpha\alpha_u + \alpha_u{}^2 + A_1A_2T_D + A_2T_D\alpha + A_2T_D\alpha_u}e^{-A_1(1+x_D)}\right) \tag{A31}$$

$$\bar{\bar{P}}_{D2} = \frac{\alpha}{s}\times\left(\frac{1}{A_1\alpha + A_1\alpha_u + 2\alpha\alpha_u + \alpha_u{}^2 + A_1A_2T_D + A_2T_D\alpha + A_2T_D\alpha_u}e^{(-A_1+A_2x_D)}\right) \tag{A32}$$

References

Ambastha, A. K., Mcleroy, P. G. & Grader, A. S. 1989. Effects of a partially communicating fault in a composite reservoir on transient pressure testing. SPE Formation Evaluation, 4 (02), 210-218.

Apps, J. A., Zheng, L., Zhang, Y., Xu, T. & Birkholzer, J. T. 2010. Evaluation of Potential Changes in Groundwater Quality in Response to CO2 Leakage from Deep Geologic Storage. Transport in Porous Media, 82 (1), 215-246.

Bense, V. F. & Person, M. A. 2006. Faults as conduit-barrier systems to fluid flow in siliciclastic sedimentary aquifers. Water Resources Research, 42 (5).

Birkholzer, J. T., Zhou, Q. & Tsang, C.-F. 2009. Large-scale impact of CO 2 storage in deep saline aquifers: a sensitivity study on pressure response in stratified systems. International Journal of Greenhouse Gas Control, 3 (2), 181-194.

Bixel, H. C., Larkin, B. K. & Vanpoollen, H. K. 1963. Effect of Linear Discontinuities on Pressure Build-up and Drawdown Behavior. Transactions of the Society of Petroleum Engineers of Aime, 228 (8), 885-895.

Caine, J. S., Evans, J. P. & Forster, C. B. 1996. Fault zone architecture and permeability structure. Geology, 24 (11), 1025-1028.

Ebigbo, A., Class, H. & Helmig, R. 2007. CO2 leakage through an abandoned well: problem-oriented benchmarks. Computational Geosciences, 11 (2), 103-115.

Humez, P., Audigane, P., Lions, J., Chiaberge, C. & Bellenfant, G. 2011. Modeling of CO 2 leakage up through an abandoned well from deep saline aquifer to shallow fresh groundwaters. Transport in Porous Media, 90 (1), 153-181.

Huntoon, P. & Lundy, D. A. 1979. Fracture-Controlled Ground-Water Circulation and Well Siting in the Vicinity of Laramie. Ground Water, 17(5) (5), 463-469.

IPCC 2005. Special Report on Carbon Dioxide Capture and Storage: Prepared by Working Group III of the Intergovernmental Panel on Climate Change. Cambridge University Press.

Maslia, M. L. & Prowell, D. C. 1990. Effect of Faults on Fluid-Flow and Chloride Contamination in a Carbonate Aquifer System. Journal of Hydrology, 115 (1-4), 1-49.

Matlab, 2015. 8.6. The MathWorks, Inc., Natick, Massachusetts, United States.

Mosaheb, M. & Zeidouni, M. Above-Zone Pressure Response to Distinguish Between Fault and Caprock Leakage. SPE Western Regional Meeting, 2017a. Society of Petroleum Engineers.

Mosaheb, M. & Zeidouni, M. Pressure Transient Analysis for Leaky Well Characterization and its Identification From Leaky Fault. SPE Health, Safety, Security, Environment, & Social Responsibility Conference-North America, 2017b. Society of Petroleum Engineers.

Pruess, K. 2005. Numerical studies of fluid leakage from a geologic disposal reservoir for CO2 show self-limiting feedback between fluid flow and heat transfer. Geophysical Research Letters, 32 (14).

Raghavan, R. 2010. A composite system with a planar interface. Journal of Petroleum Science and Engineering, 70(3), 229-234.

Rahman, N. M., Miller, M. D. & Mattar, L. 2003. Analytical solution to the transient-flow problems for a well located near a finite-conductivity fault in composite reservoirs. In SPE Annual Technical Conference and Exhibition.

Shakiba, M. & Hosseini, S. A. 2016. Detection and characterization of CO 2 leakage by multi-well pulse testing and diffusivity tomography maps. International Journal of Greenhouse Gas Control, 54, 15-28.

Shan, C., Javandel, I. & Witherspoon, P. A. 1995. Characterization of leaky faults: Study of water flow in aquifer-fault-aquifer systems. Water Resources Research, 31(12), 2897-2904.

Sibson, R. 1977. Fault rocks and fault mechanisms. Journal of the Geological Society, 133 (3), 191-213

Stehfest, H. 1970. Algorithm 368: Numerical inversion of Laplace transforms [D5]. Communications of the ACM, 13 (1), 47-49.

Stewart, G. & Gupta, A. 1984. The interpretation of interference tests in a reservoir with sealing and partially communicating faults. European Petroleum Conference.

Stoessell, R. K. & Prochaska, L. C. 2005. Chemical evidence for migration of deep formation fluids into shallow aquifers in south Louisiana. Gulf Coast Association of Geological Sciences Transactions, 794-808.

Thomas, D. C. & Benson, S. M. 2005. Carbon dioxide capture for storage in deep geologic formations, Elsevier.

Yaxley, L. M. 1987. Effect of a partially communicating fault on transient pressure behavior. SPE Formation Evaluation, 2(04), 590-598.

Zeidouni, M. 2012. Analytical model of leakage through fault to overlying formations. Water Resources Research, 48.

Zeidouni, M. 2016. Semi-Analytical Model of Pressure Perturbations Induced by Fault Leakage in Multilayer System. Journal of Hydrologic Engineering, 21 (6).

Zeidouni, M. & Pooladi-Darvish, M. 2012. Leakage characterization through above-zone pressure monitoring: 1—Inversion approach. Journal of Petroleum Science and Engineering, 98, 95-106.